

Supporting Information

Imaging of the nuclei of tumor cells by novel ruthenium(II) complexes coordinated with 6-chloro-5-hydroxypyrido[3,2-a]phenazine

Yang Ding¹, Qiong Wu¹, Kangdi Zheng², Linkun An^{3*}, Xiaoying Hu¹, Wenjie Mei^{1*}

Table of contents:

1. Synthesis characterization of ruthenium(II) complexes **1** and **2**
 - 1.1 Synthetic route of two novel complexes **1** and **2**.
 - 1.2 Reaction of profile of ruthenium(II) complexes **1** and **2** in ethanol irradiated by microwave for 30 min.
 - 1.3 The ¹H NMR spectra of DCQ.
 - 1.4 The ESI-MS spectra of **1** and **2**.
 - 1.5 The ESI-MS spectra of CQM.
 - 1.6 The ¹H NMR spectra of **1** and **2**.
 - 1.7 The ¹³C NMR spectra of **1** and **2**.
2. The concentration change in UV-Vis absorbance of the complexes **1** and **2** in the cultivation media cell with time passed up to 6 h, (A) and (B) in HepG2 cell; (C) and (D) in HeLa cell; (E) and (F) in MCF-7 cell.

3. The cellular uptake of complexes **1** and **2** by UV-vis absorbance standard curve.
4. Photophysical data of complexes **1** and **2**.
5. Photophysical properties of DAPI, Hoechst 33258, and complexes **1** and **2**.
6. Photostability assay of complexes **1** and **2**.
7. Interaction of complexes **1** and **2** with biomolecules.

1.3 The ^1H NMR spectra of DCQ

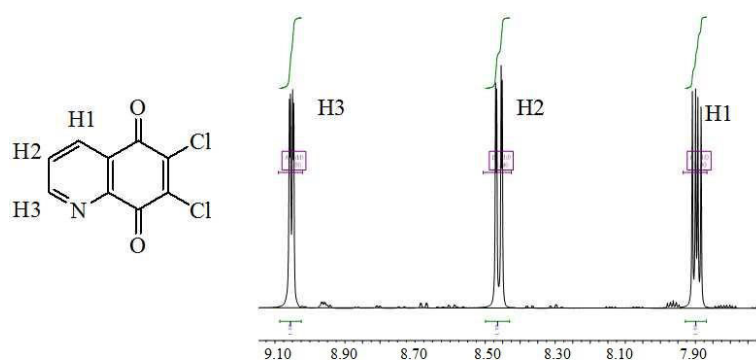


Figure. S3 The ^1H NMR spectra of DCQ.

1.4 The ESI-MS spectra of CQM

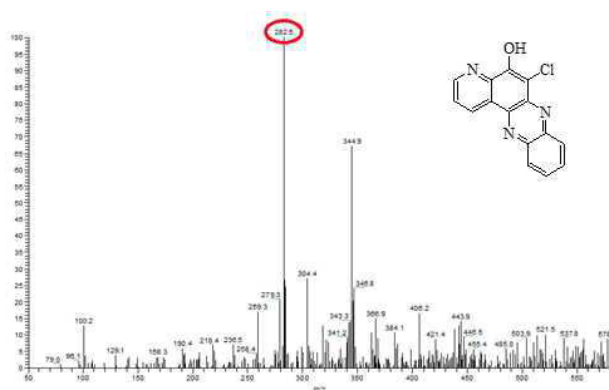


Figure. S4 The ESI-MS spectra of CQM.

1.5 The ESI-MS spectra of 1 and 2

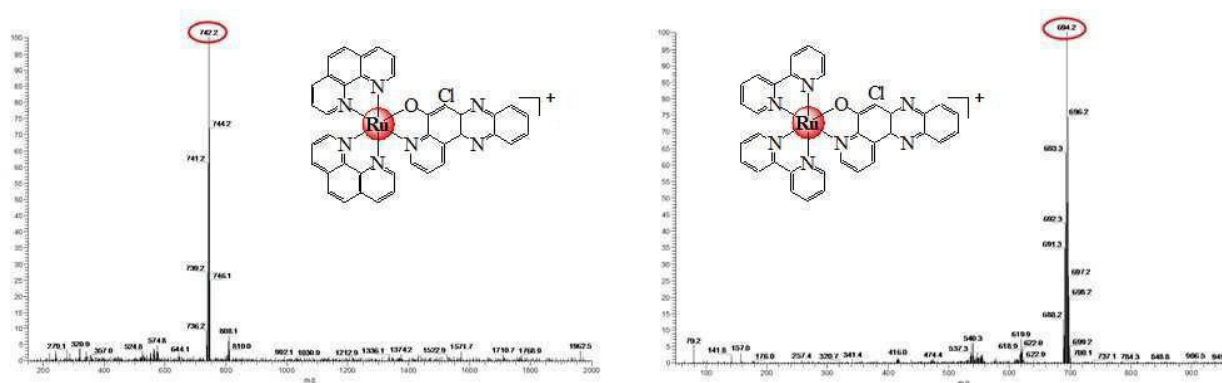


Figure. S5 The ESI-MS spectra of 1 and 2.

1.6 The ^1H NMR spectra of **1** and **2**

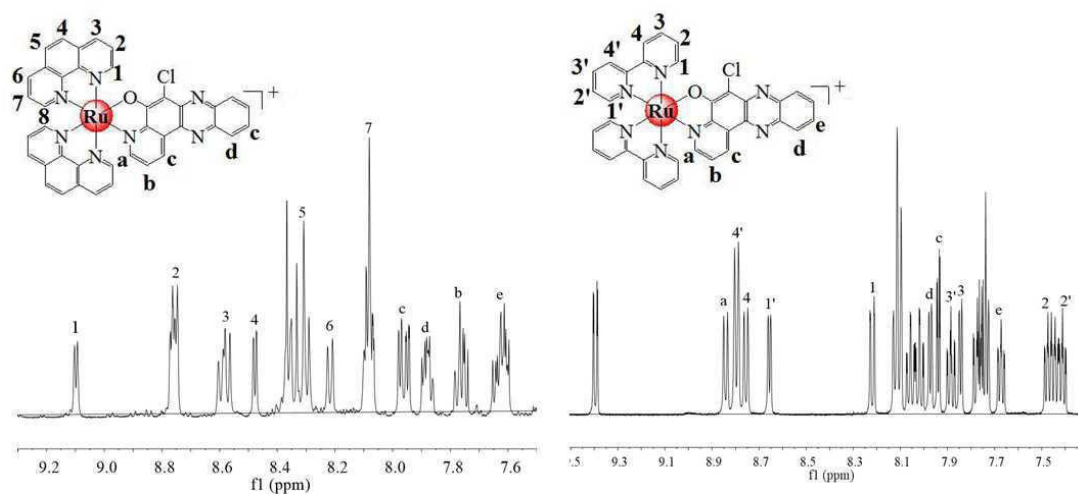


Figure. S6 The ^1H NMR spectra of **1** and **2**.

1.7 The ^{13}C NMR spectra of **1** and **2**

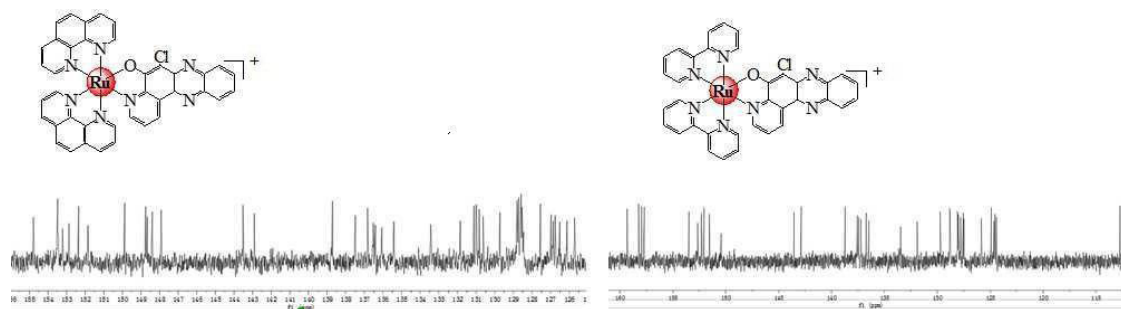


Figure. S7 The ^{13}C NMR spectra of **1** and **2**.

2. The concentration change in UV-Vis absorbance of the complexes 1 and 2

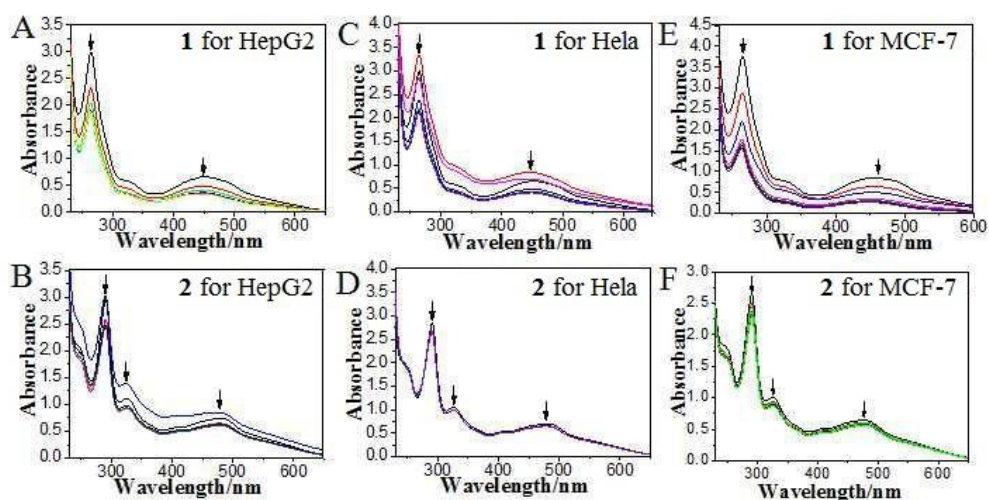


Figure S8. The concentration change in UV-Vis absorbance of the complexes 1 and 2 in the cultivation media cell with time passed up to 6 h, (A) and (B) in HepG2 cell; (C) and (D) in HeLa cell; (E) and (F) in MCF-7 cell.

3. The cellular uptake of complexes 1 and 2 by UV-vis absorbance standard curve

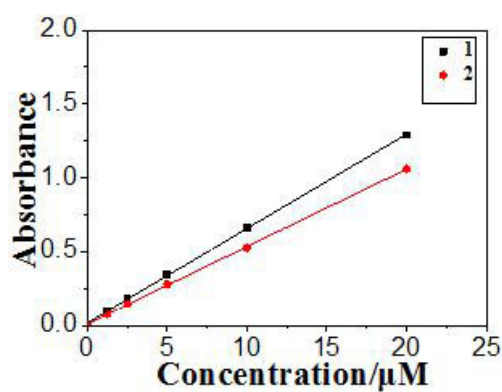


Figure S9. The cellular uptake of complexes 1 and 2 by UV-vis absorbance standard curve.

4. Photophysical data of complexes **1** and **2**

Table 1. Photophysical data of complexes **1** and **2**

Complex	λ_{em} (nm)	Quantum yield (%)	Extinction coefficient ($M^{-1}\cdot cm^{-1}$) (calculated based on MLCT absorbance)	Extinction coefficient ($M^{-1}\cdot cm^{-1}$) (calculated based on IL absorbance)	Brightness ^a
1	580	1.34	4.6×10^4	9.8×10^3	62
1+BSA		1.54			71
2	579	0.12	2.6×10^4	6.4×10^3	3
2+BSA		0.17			4

Note: ^aBrightness of complex **1** and **2**, (extinction coefficient \times quantum yield)/1000. Ruthenium(II) complex **1** and **2** (25 μ M) was mixed with BSA (16 μ M), the quantum yield of the adduct of Ruthenium(II) complexes **1** and **2** with BSA were measured, respectively.

5. Photophysical properties of DAPI, Hoechst 33258, and complexes **1** and **2**

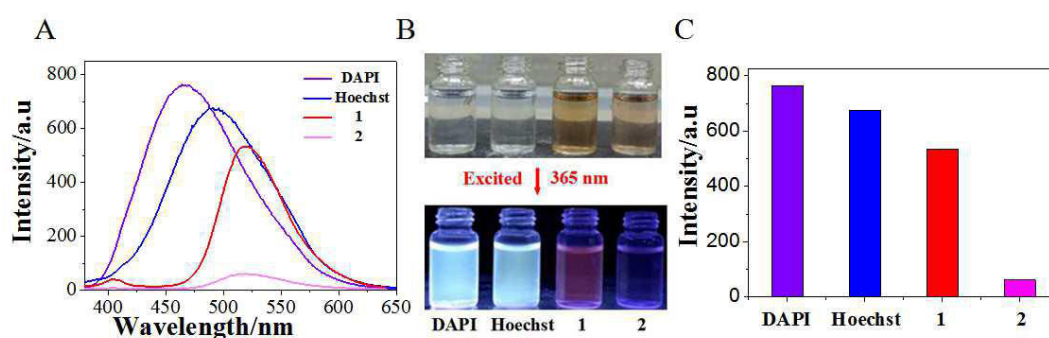


Figure S10. (A) Emission spectra of DAPI, Hoechst 33258, **1** and **2** in PBS buffer solution (pH 7.2), excited by 365 nm. (B) Fluorescence of **1** and **2** in PBS buffer solution (pH 7.2) excited at 365 nm from a portable lamp; (C) Fluorescence intensity

of DAPI, Hoechst 33258, **1** and **2** in PBS buffer solution (pH 7.2). [Ru] = 25 μ M.

[DAPI]= 25 μ M, [Hoechst 33258]= 25 μ M, [Ru] = 25 μ M.

6. Photo-stability assay of complexes **1** and **2**

The **1**, **2**, DAPI and Hoechst 33258 (25 μ M) were dissolved in PBS buffer solution (pH 7.2). The Photostability assay of solutions were carried out illuminating an spectrophotometric quartz cell of 1-cm path length. The light source was a portable lamp 365 nm portable lamp. Luminescent spectra were measured with RF-5301 fluorescence spectrophotometer. Samples were irradiated for appropriate times, the emission intensity was measured in the fluorometer. When aqueous solutions of **1**, **2**, DAPI and Hoechst 33258 were irradiated with portable lamp, spectral changes were observed (Fig. S11). The maximal intensity of **1**, **2**, DAPI and Hoechst 33258 were at 580, 579, 465 and 487 nm, and no alteration of the luminescent spectrum was detected after irradiation (Fig S11. A–D). It's found that the fluorescence intensity of **1**, **2**, DAPI and Hoechst 33258 decreased gradually, especially DAPI decreased almost 35% after two hours, which complexes **1** and **2** generally presented lower quench rate than DAPI. All above results indicated that the complex **1** exhibited considerable

emission and greater photo-stability compared with commercial dye DAPI and Hoechst 33258.

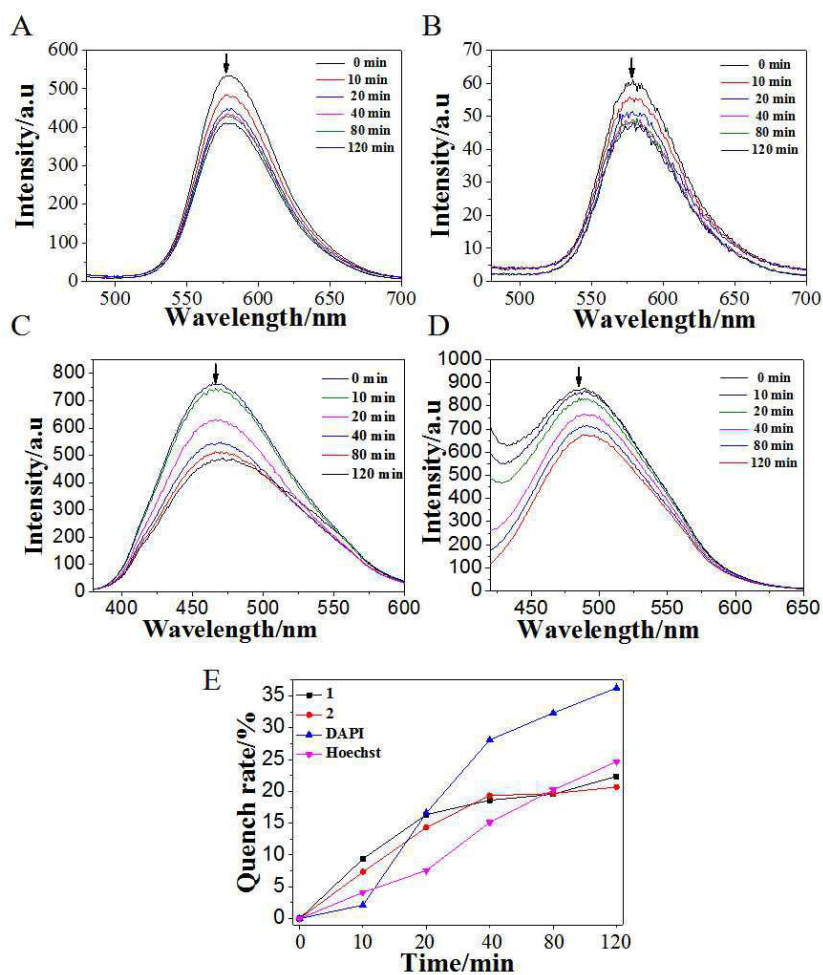


Figure S11. Changes of electronic spectral of **1**, **2**, DAPI and Hoechst 33258 in PBS buffer solution (pH 7.2) following the time course (A–D). Specific conditions are labeled on the graphs. Irradiation times is 0, 10, 20, 40, 80 and 120 min. [DAPI]= 25 μ M, [Hoechst 33258]= 25 μ M, [Ru] = 25 μ M; The time course quench rate of **1**, **2**, DAPI and Hoechst 33258 irradiation by portable lamp (E).

7. Interaction of complexes **1** and **2** with biomolecules

The interaction of complexes **1** and **2** with bovine serum albumin (BSA) and CT-DNA have been investigated by luminescent emission titration and electronic absorption titrations. The results show that both **1** and **2** exhibited stronger affinity to BSA than CT-DNA. This is confirmed by the obviously hypochromism in the characterized IL absorption of both complexes in the presence of BSA and relatively subtle changes in the presence of CT-DNA. With the increase of BSA, the IL absorption of complex **1** and **2** exhibited hypochromism of about 18.3 and 12.3%, respectively (Fig S12. a–b). However, with the increase of CT-DNA, the IL absorption of complex **1** and **2** exhibited hypochromism of about 12.7 and 11.7%, respectively (Fig S12. c–d). Moreover, fluorescence titration experiments of complexes **1** and **2** (25 μ M) with BSA and CT-DNA in buffer solution were performed. With the increase of BSA, the emission intensity of complexes **1** and **2** were increased notably, which were about 1.32 and 1.30 times larger than in the absence of BSA, respectively (Fig S12. A–B). However, with the increase of CT-DNA, the emission intensity of complexes **1** and **2** kept almost no change (Fig S12. C–D). These results indicated that Ru complex exhibit stronger affinity to protein than DNA, but

the detailed mechanism for the nucleus staining by the Ru complex still need further research.

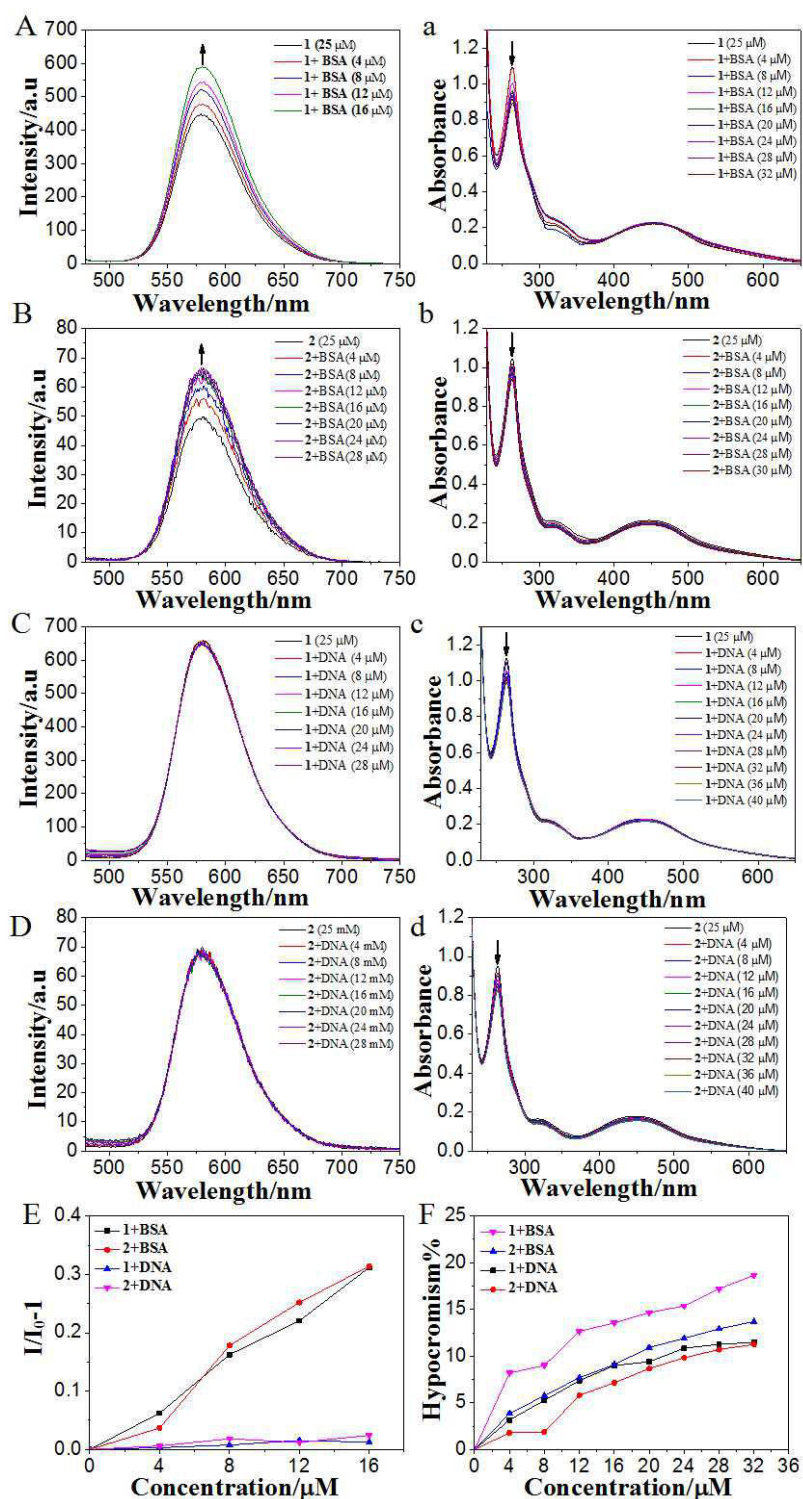


Figure S12. Emission spectra of complexes **1** and **2** in PBS buffer in the absence and presence of BSA (A–B); Emission spectra of complexes **1** and **2** in Tris–HCl buffer in

the absence and presence of CT-DNA (C–D); Absorption spectra of complexes in PBS buffer upon addition of BSA in the presence of complexes **1** and **2** (a–b); Absorption spectra of complexes in PBS buffer upon addition of CT-DNA in the presence of complexes **1** and **2** (c–d). [Ru] = 25 μ M. Arrow shows the intensity change upon increasing BSA / CT-DNA concentrations; The change of intensity of complexes **1** and **2** with the increase of BSA / CT-DNA was compared (E); The change of hypochroism of complexes **1** and **2** with the increase of BSA / CT-DNA was compared (F).